Journal of Engineering and Applied Sciences 9 (1): 6-11, 2014
ISSN: 1816-949X

Wetting of Thermally Grown Oxide Layer on the C36000 Copper Alloy Surfaces

Aniedi Nyong and Pradeep Rohatgi
Department of Materials Engineering, University of Wisconsin-Milwaukee,
Milwaukee, WI 53201, United States

Abstract: Thermal oxidation of C36000 copper alloy in N_2-5 wt. % O_2 and N_2-12 wt. % O_2 was used to grow nanowires on the surfaces of the substrate. Energy dispersive X-ray analysis of the nanowires confirmed their composition as ZnO. The dimensions of the ZnO nanowires, as well as the thickness of the oxide layer varied with the thermal oxidation parameters of time and weight percentage of oxygen. The measured contact angles of water drops on the surfaces of these samples showed a dependency on the values of the fractional surface area of the ZnO nanowires as well as on the oxide layer thickness. An anti-wetting surface with water contact angle of 142° was obtained after 2 h of thermal oxidation of the C36000 copper alloy in N_2-12 wt. % O_2, corresponding to a Cassie-Baxter wetting state with growth of ZnO nanowires on convoluted oxide layer.

Key words: Oxide, nanowires, wenzel, cassie-baxter, wetting, copper alloy

INTRODUCTION

The effect of changes in the surface morphology on the wetting behavior of water on thermally oxidized C36000 copper alloy through the growth of oxide nanowires on the oxide layer has not been studied prior to now. The C36000 copper alloy has enormous use in plumbing (Damodar *et al*., 2009) where it is exposed to water. This provides a strong need to understand the effect of changes in the morphology, created through the cheap route of thermal oxidation, on their wettability to water.

The factors that affect the wettability of surfaces have been established. These include the roughness and chemical nature of the surfaces. Various models have been developed to explain the relationship between the surfaces and the observed contact angles of liquids. Two of these models, the Wenzel (Liu and Jiang, 2011) and the Cassie-Baxter (Quere, 2008) models have however been effective. The Wenzel model suggests that a liquid drop placed on a rough surface fills the rough grooves. The Cassie-Baxter model, on the other hand assumes that the liquid drop does not have full contact with the surface due to the trapping of air bubbles in the rough grooves of the surface.

The contact angle of water droplet modified for the roughness of the surface based on the Wenzel model is given by Eq. 1:

$$\cos\theta^{*} = r_f \cos\theta \quad (1)$$

In Eq. 1, r_f is the roughness factor which is the ratio of the actual area of the rough surfaces to the projected area (Borras and Gonzalez-Elipe, 2010). For the Cassie-Baxter case, the fraction of the liquid drop in contact with the solid surfaces, f_{sl} is introduced and the contact angle is given by Eq. 2:

$$\cos\theta_{CB} = f_{sl}(1+\cos\theta)-1 \quad (2)$$

Based on these models, considerable research effort has been directed to the modification of the texture of metals in order to achieve very high contact angles for water and oil for self-cleaning (Zhang and Lamb, 2009) and anti-fouling applications (Yang *et al*., 2012).

The synthesis of nanowires on copper alloys has been possible through a direct thermal oxidation process with specific interest mostly directed to solid state applications of such wires.

Recently however, a commercial aluminum alloy has been thermally oxidized in air to create a rough surface on which wettability was studied (Samad and Nychka, 2011). In the same vein, super hydrophobicity has been achieved on a pure copper substrate by the growth of CuO nanowires through a thermal oxidation-reduction route (Seung-Mo *et al*., 2012).

In this study, researchers report the effects of changes of the surface morphology on the wetting behavior of water drops on thermally oxidized leaded C36000 copper alloy samples. The surface morphology is controlled by the growth of nanowires of various dimensions on a convoluted oxide layer under different conditions of time and weight composition of oxygen in the oxidizing gas mixture.

Corresponding Author: Aniedi Nyong, Department of Materials Engineering, University of Wisconsin-Milwaukee, Milwaukee, WI 53201, United States

MATERIALS AND METHODS

The materials used for the experiments included the C36000 copper alloy obtained from Badger meter in Milwaukee, Wisconsin, USA. The chemical composition is as stated in Table 1.

The different Nitrogen-Oxygen gas mixtures used for the experiments were N_2-5 wt. % O_2 and N_2-12 wt. % O_2 gas mixtures obtained from Praxair. The choice of these gas mixtures is to effect varying oxygen concentration within the furnace during the thermal oxidation process.

Experimental method: The copper alloy sample was sectioned into 25×5×3 mm pieces. These were then polished until fine surfaces were obtained by using a soft cloth impregnated with 1 μm alumina. The polished samples were washed with distilled water to remove dirt and the dried. The samples were then placed in a furnace and heated to a temperature of 650°C. The concentration of oxygen during the thermal oxidation process was controlled by the flowing the various N_2-5 wt. % O_2 and N_2-12 wt. % O_2 gas mixtures through the furnace chamber at a flow rate of 4.5 L min^{-1} at 1 a.m. The process was carried for different time duration of 1-3 h. After the set time, the samples were cooled in an evacuated bell jar to cool. For oxide layer thickness measurement, the sides of the samples were polished after the thermal oxidation process to reveal the oxide layer for thickness evaluation.

Characterization technique: The average surface roughness, Ra, of both the polished and thermally oxidized samples was measured using a Phase II SRG-450 2-D surface profilometer. The average of 5 readings of the Ra values taken at 5 different spots on the samples surfaces was taken. The contact angles of water on these prepared surfaces were measured at room temperature using a Rame Hart 250 model contact angle goniometer. About 5 drops of about 5 μL of distilled water were placed on five different locations on the surfaces of the samples and the average value taken for the contact angle. The surface morphology, thickness of the oxide layer and the chemical composition of the surface features were evaluated with the Hitachi-S4800 Scanning Electron Microscope; equipped with the energy dispersive X-ray analytical tool. Also, the 2000-scintag X-ray diffractometer ($Cu K_\alpha$ radiation, λ = 1.5406°A) was used in determining oxidation products formed due to the thermal oxidation. The X-ray diffraction studies were done for a 2θ range of 25-70° at a constant scan rate of 2.00° min^{-1}.

Table 1: The chemical composition of C36000 copper alloy

Elements	Nominal wt. (%)
Cu	61.50
Fe	0.35
Pb	3.00
Zn	35.40

RESULTS AND DISCUSSION

The measured cross-sectional thickness of the oxide layers as seen in Fig. 1 showed that there was a substantial growth of the layer on the samples during the thermal oxidation process. The values of the average thickness of these layers increased with the time set for the thermal oxidation process, as stated in Table 2. However after 3 h of the process, the average oxide layer showed no further increase in the thickness for samples oxidized with N_2-12 wt. % O_2 oxidizing gas mixture.

Though, the rate of the growth of the oxide layer increased initially, the lack of further increase in the thickness of the oxide layer after 3 h of thermal oxidation in N_2-12 wt. % O_2 gas mixture is due to the inhibition of the diffusion of the reactive oxygen species through the oxide layer after a period of time. This behavior agrees with the parabolic law that governs the high temperature thermal oxidation of copper alloys (Hu *et al*., 2011).

The resulting oxidation kinetic plots for the growth of the oxide layers are shown in Fig. 2, for the variation of oxide layer thickness (X) with the square root of the thermal oxidation time ($t^{1/2}$) at 650°C in air and the N_2-O_2 oxidizing gas mixtures.

The surfaces of the oxide layer in the SEM images in Fig. 3 showed distortion and convolution. During the growth of the oxide layer, growth stresses are generated. Most of the growth stresses are from the differences in the volume of the oxides formed and the consumed substrate which is explained by the Pilling-Bedworth ratio (Qian and Shen, 2005). These growth stresses may be relieved through plastic deformation which may occur in the oxide layer or in the brass alloy. Considering the melting points of the C36000 brass (887.8°C) and the oxides, the plastic deformation of the brass substrate will be easier than the oxides. However, due to the thinness of the oxide layer, the plastic deformation occurs in the oxide layer under compressive stresses resulting in the convolution of these layers (Kumar *et al*., 2004).

Beyond the convolution of the oxide layer, as observed in Fig. 3, nanowires were found to grow randomly on the oxide layer within certain window of time during the thermal oxidation of the samples in the two gas mixtures used in the process. The average lengths, average cross sectional diameters and the average distances between the oxide nanowires were evaluated from the SEM images. As stated in Table 2, increase in the weight percentage of oxygen in the oxidizing gas mixture

Table 2: Dimensions of ZnO nanowires/oxide layer, f_{sl} and θ_{water}

Gas mixture	Time (h)	R_a	Average diameter	Average length	Distance b/w nanowires	Average thickness	f_{sl}	f_{sl}	θ_{water}
No oxidation	0	0.10							53°±2°
N_2-5 wt. % O_2	1	0.10				30.3±3.1			85°±6°
	2	0.34	27±0.01	0.20±0.04	0.23±0.09	47.7±1.7		0.68	124°±2°
	3	0.43	35±0.01	0.23±0.09	0.24±0.10	48.3±1.9	0.002	0.27	116°±8°
N_2-12 wt. % O_2	1	0.63	29±0.01	0.36±0.13	0.19±0.07	44.7±8.4	0.017	0.35	132°±3°
	2	0.40	58±0.01	0.40±0.23	0.30±0.15	56.8±2.1	0.015	0.21	142°±3°
	3	0.65				24.5±1.6		0.14	38°±11°

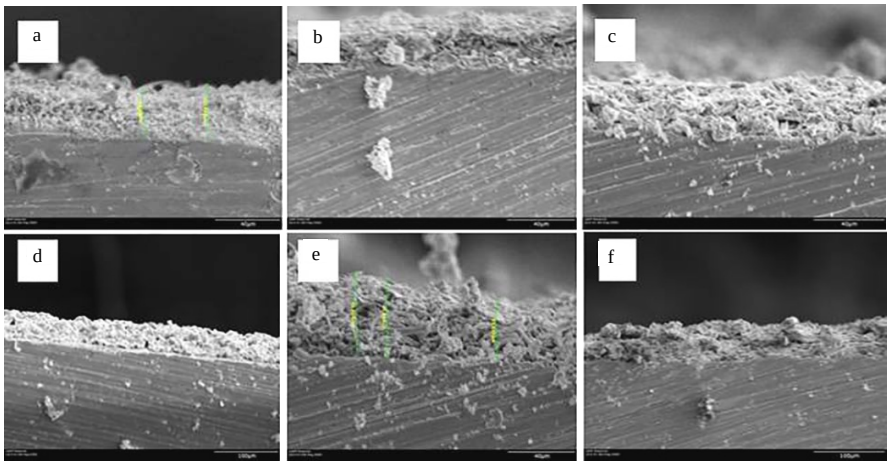

Fig. 1: A cross-section showing the thickness of the oxide layer; a) 1 h in N_2-5 wt. % O_2; b) 2 h in N_2-5 wt. % O_2; c) 3 h in N_2-5 wt. % O_2; d) 1 h in N_2-12 wt. % O_2; e) 2 h in N_2-12 wt. % O_2; f) 3 h in N_2-12 wt. % O_2

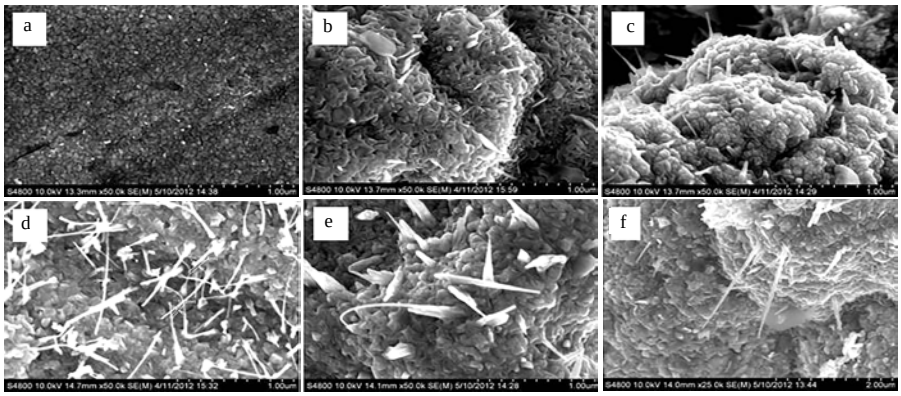

Fig. 2: SEM images of thermally oxidized C36000 copper alloy showing oxide layer convolution and ZnO nanowire growth: a) 1 h in N_2-5 wt. % O_2; b) 2 h in N_2-5 wt. % O_2; c) 3 h in N_2-5 wt. % O_2; d) 1 h in N_2-12 wt. % O_2; e) 2 h in N_2-12 wt. % O_2; f) 3 h in N_2-12 wt. % O_2

resulted in an increase in the average lengths and diameters of the resulting nanowires. These increases in dimensions are simply due to the availability of more oxygen to drive the growth of the oxide nanowires (Xu *et al*., 2011a, b). Equally, the average length and diameter of the nanowires was found to increase with time. It was obvious that there was an optimum time for the growth of the nanowires in the N_2-O_2 gas mixtures at the prevailing temperature. The X-ray diffraction patterns for the oxide layers for samples thermally oxidized in N_2-5 wt. % O_2 and N_2-12 wt. % O_2 gas mixtures are shown in Fig. 4a, b.

In the N_2-5 wt. % O_2 and N_2-12 wt. % O_2 the major diffraction peaks corresponded to various planes of Zinc Oxide (ZnO) and lead oxide (PbO) as shown in Fig. 4a, b. Lead is present as a low melting (327.5°C)

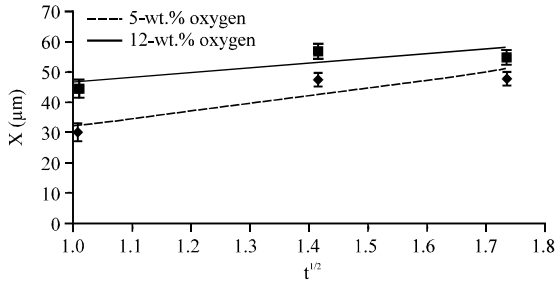

Fig. 3: Plot of the oxide layer thickness (X) against the square root of the thermal oxidation time (t)

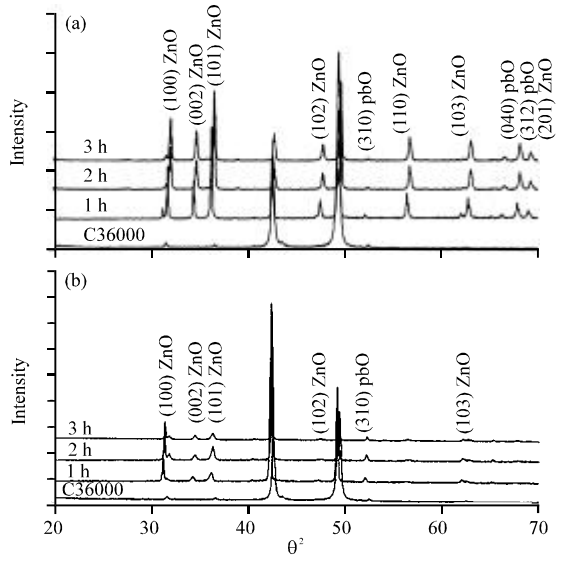

Fig. 4: a) X-ray diffraction pattern of C36000 copper alloy thermally oxidized in N_2-5 wt. % O_2 gas mixture; b) X-ray diffraction pattern of C36000 copper alloy thermally oxidized in N_2-12 wt. % O_2 gas mixture

alloying component in the C36000 copper alloy was oxidized to PbO due to the relative ease of melting and segregation on the sample surfaces. These observed planes corresponded to those of the diffraction pattern of ZnO and PbO in PDF cards number 36-1451 and 38-1477, respectively. All the peaks for the ZnO formed on the surfaces of the samples in both N_2-O_2 oxidizing gaseous mixtures confirm a hexagonal ZnO crystal structure. Also, the preponderance of the ZnO diffraction peaks confirmed that the oxide layer is mainly composed of ZnO as a continuous layer.

It should be noted that the formation of an external ZnO layer on the oxidation of copper-zinc alloys depend on the critical concentration of zinc in the alloy (Wagner, 1959). If the zinc concentration is lower than the critical concentration, internal oxidation will occur resulting in the absence of an external, continuous zinc oxide layer. The concentration of the zinc in the C36000 copper alloy is above that critical zinc concentration in the alloy, hence the formation of the external ZnO layer. To confirm the chemical composition of the oxide nanowires formed, an energy dispersive X-ray analysis was done on the nanowires. The energy dispersive X-ray analysis of the nanowires showed that the Zn and O atoms were in a relative weight percent of 80.47 and 19.53 wt. %, respectively. This confirms that the nanowires are composed of zinc oxide. The formation of the ZnO nanowires can be explained on the basis of a simple mechanism involving the steps of nucleation and growth (Wang, 2004). At the temperature used in the thermal oxidation, the zinc phase in the samples melts and segregates on the surface providing favorable sites for the adsorption of oxygen atoms and subsequent oxidation of the zinc to zinc oxide nuclei. The ZnO nanowires grow from these zinc oxide nuclei formed on the surfaces of the samples.

The average surface roughness, R_a and the average contact angles of water measured on these surfaces are presented in Table 2. It was observed that the average surface roughness was higher on surfaces that had ZnO nanowires. The presence of the ZnO nanowires sufficiently altered the surface morphologies which resulted in increased surface roughness. Therefore, the samples oxidized in N_2-12 wt. % O_2 were rougher than those oxidized in N_2-5 wt. % O_2 in the time instances that had the growth of the ZnO nanowires. This is due to the formation of longer and thicker nanowires on equally thicker oxide layers in the N_2-12 wt. % O_2 when compared to the N_2 5 wt. % O_2 gas mixtures. It is expected that these changes in the thickness of the convoluted oxide layer and dimension of the ZnO nanowires will affect the wetting behavior and contact angle of water on the surfaces. In terms of the average contact angle of water on these surfaces, there was a sharp increase in the measured values on surfaces with the ZnO nanowires growing on the oxide layer, as stated in Table 2. The high values of 124° and 142° for contact angles of water were observed for the C36000 copper alloy samples thermally oxidized at 2 h in N_2-5 wt. % O_2 and N_2-12 wt. % O_2 oxidizing gas mixtures. The reduction in the ZnO layer thickness and lack of growth of ZnO nanowires resulted in low values of the contact angles of water, as seen with the surface of samples thermally oxidized for 1 and 3 h in N_2-5 wt. % O_2 and N_2-12 wt. % O_2 gas mixtures, respectively.

The oxide layers that exhibited this strong water repellence also had the ZnO nanowires growing on them. These water repelling oxidized surface layers beyond the growth of ZnO were reasonably thick with values >30 microns. In order to correlate the wettability to the surface morphologies generated during the process of thermal oxidation, the average diameters and the average distances between the ZnO nanowire were used to estimate the water-solid fractional area, f_{sl} for the drop of water sitting on these sample surfaces. The f_{sl} in this case is given by the ratio:

$$f_{sl} = \frac{A_{sl}}{A_{proj}} \quad (3)$$

Where:

A_{sl} = The area of the solid-liquid interface

A_{proj} = The projected area from which the ZnO nanowires grow

Researchers assume that the nanowires are cylindrical with circular tips of average diameter, D, growing from a circular plane of projection of radius, X and separated from each other by a distance of 2X (Fig. 5). Based on the ratio stated in Eq. 3, researchers have that.

Since, D+2X is approximately equal to 2X because of the very small values of D then the f_{sl} is approximated as Eq. 4:

$$f_{sl} = \frac{\pi\left(\frac{D}{2}\right)^2}{\pi\left[\frac{D+2X}{2}\right]^2} \quad (4)$$

$$f_{sl} = \frac{D^2}{(D+2X)^2} \quad (5)$$

Using this expression, the calculated f_{sl} for the surfaces with the ZnO nanowires were all very low, <<1. Following Eq. 3, the f_{sl} values obtained for the Cassie-Baxter wetting state were of higher values compared to the f_{sl} values calculated from Eq. 6.

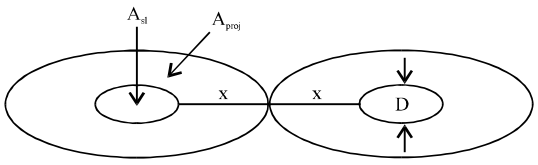

Fig. 5: ZnO nanowire growing from a plane of projection of an oxide layer

$$f_{sl} = \left(\frac{D}{2X}\right)^2 \quad (6)$$

This only suggests that beyond the ZnO nanowires, the thickness of the ZnO layer oxide layer has contributed to the interface between the water drop and the solid surface. It is expected that increase in the surface roughness, as given by the average roughness parameter, R_a should result in a decrease in the observed contact angle of water for a hydrophilic metallic surface. In this case, however the increase in surface roughness due to the growth of the ZnO nanowires of different sizes was equally accompanied with an increase in the thickness of the oxide layer formed at the 2 and 3 h in N_2-5 wt. % O_2 and at 1 and 2 h in N_2-12 wt. % O_2 gas mixtures, respectively. Air trapped within the grooves of the convoluted oxide layer caused an increase in the air/water interface, preventing the water drops from penetrating the grooves of the oxidized surface.

This shifts the behavior of the surface towards hydrophobic, non-wetting behavior and the increase in the surface roughness due to the growth of the ZnO nanowires rather than lead to a reduction in the contact angles of water accentuates them. The high contact angles observed due to the combination of the ZnO nanowires and the oxide layer grooves correspond to the Cassie-Baxter wetting state. The very low values obtained for the fractional surface area available for the wetting of the water drops on the surfaces on which the ZnO nanowires grew means that the fraction of the surface for the liquid-air interface is sufficiently large enough to make these surfaces water repellent.

CONCLUSION

ZnO nanowires of various sizes were successfully grown through thermal oxidation on C36000 brass substrate. The sizes of the ZnO nanowires and the thickness of the oxide layer on which they grew varied with the thermal oxidation parameters of time and oxygen weight percent in the oxidizing gas mixture. High contact angle of water drops, corresponding to the Cassie-Baxter wetting state were measured on the surfaces that had ZnO nanowires growing on them. This was because of the small fraction of the solid-liquid interface due to the presence of the ZnO nanowires and also on the presence of air-trapping grooves, in the convoluted oxide layer on the surfaces. The shift in wetting behavior of the water drops from the hydrophilic, Wenzel state to the anti-wetting, Cassie-Baxter state was controlled by the ZnO nanowires and the thickness of the oxide layer.

ACKNOWLEDGEMENTS

This research was partially supported by National Science Foundation Industry/University Cooperative Research Center on Water Equipment and Policy located at University of Wisconsin-Milwaukee and Marquette University (IIP-0968887 and IIP-0968844). The researchers also thank Dr. Steven Hardcastle and Dr. Benjamin Schultz for their assistance.

REFERENCES

Borras, A. and A.R. Gonzalez-Elipe, 2010. Wetting properties of polycrystalline TiO_2 surfaces: A scaling approach to the roughness factors. Langmuir, 26: 15875-15882.

Damodar, R.A., S. You and H.H. Chou, 2009. Study the self cleaning, antibacterial and photocatalytic properties of TiO_2 entrapped PVDF membranes. J. Hazard. Mater., 172: 1321-1328.

Kumar, A., A.K. Srivastava, P. Tiwari and R.V. Nandedkar, 2004. The effect of growth parameters on the aspect ratio and number density of CuO nanorods. J. Phys.: Condens. Matter, 16: 8531-8543.

Liu, K. and L. Jiang, 2011. Metallic surfaces with special wettability. Nanoscale, 3: 825-838.

Qian, B. and Z. Shen, 2005. Fabrication of superhydrophobic surfaces by dislocation-selective chemical etching on aluminum, copper and zinc substrates. Langmuir, 21: 9007-9009.

Quere, D., 2008. Wetting and roughness. Ann. Rev. Mater. Res., 38: 71-99.

Samad, J.E. and J.A. Nychka, 2011. Wettability of biomimetic thermally grown aluminum oxide coatings. Bioinspir. Biomim., Vol. 6. 10.1088/1748-3182/6/1/016004

Seung-Mo, L., K. Kwang-Seop, P. Eckhard, K. Sangmin, K. Jae-Hyun and L. Hak-Joo, 2012. Facile route toward mechanically stable superhydrophobic copper using oxidation-reduction induced morphology changes. J. Phys. Chem. C, 116: 2781-2790.

Wagner, C., 1959. Types of reactions in the oxidation of Alloys. J. Electrochem. Soc., 63: 771-775.

Wang, Z.L., 2004. Zinc oxide nanostructures: Growth, properties and applications. J. Phy.: Condens. Matter., 16: 829-858.

Xu, C.H., Y.L. Liu and S.Q. Shi, 2011a. Isothermal oxidation behavior of Cu-38at.%Zn alloy at high temperature. High Temp. Mater. Proc., 30: 267-272.

Xu, C.H., Z.B. Zhu, H.F. Lui, C. Surya and S.Q. Shi, 2011b. The effect of oxygen partial pressure on the growth of ZnO nanostructure on $Cu_{0.62}Zn_{0.38}$ brass during thermal oxidation. Superlattices Microstruct., 4: 408-415.

Yang, J., Z. Zhang, X. Xu, X. Zhu, X. Men and X. Zhou, 2012. Superhydrophilic-superoleophobic coatings. J. Mater. Chem., 22: 2834-2837.

Zhang, H. and R.N. Lamb, 2009. Superhydrophobic treatment for textiles via engineering nanotextured silica/polysiloxane hybrid material onto fibres. Surf. Eng., 25: 21-24.